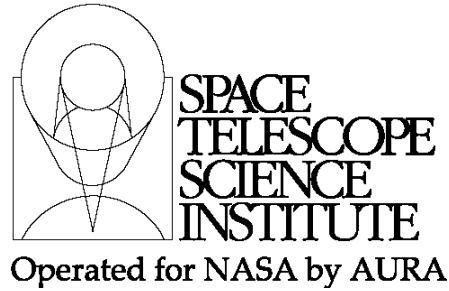




TECHNICAL MEMORANDUM



Title: Algorithms for Transforming GSC-II Magnitudes into the NIR	Doc #: JWST-STScI-001410
	Date: April 14, 2008
	Rev: -
Authors: Pierre Chayer & Edmund P. Nelan	Phone: 410-338-5097
	Release Date: 7 May 2008

1.0 Abstract

The Science & Operation Center (S&OC) will use the Guide Star Catalog-II (GSC-II) for selecting JWST guide stars and their associated reference stars. The GSC-II is derived from an all-sky survey in three optical passbands. However, because JWST's FGS-Guider is a near infrared camera, the GSC-II magnitudes must be transformed into the near-infrared pass bands, and ultimately into the expected electron count rates at the Guider's detector, to support JWST operations. In this report we propose algorithms for transforming the GSC-II magnitudes into the NIR J , H , and K_s system. These algorithms have been derived and calibrated using the 2MASS point source catalog for regions of the sky at high Galactic latitude where reddening is minimal and nearly uniform. We find that the transformations derived in this manner may not be applicable for observations in the disk of the Galaxy where extinction and reddening can be substantial and locally variable.

2.0 Introduction

The Fine Guidance Sensor-Guider (FGS-Guider) is a near-infrared (NIR) camera that measures the position of a guide star on its detector. After a slew to a new target field, the Observatory Scripts Subsystem (hereafter referred to as the "onboard scripts") command the FGS-Guider to perform a series of functions (Identification, Acquisition, Track, and Fine Guide) that ultimately provide data for stabilizing and fine guiding the observatory. To facilitate the successful execution of these functions, the scripts provide the FGS-Guider flight software (FSW) with the predicted electron count rate (brightness) of the guide star and several reference stars (which are needed by the Identification function). The ground system, in turn, provides these count rates (along with positional data) to the onboard scripts.

The reference and guide stars are selected from the Guide Star Catalog-II (GSC-II), which is the deepest all-sky survey available (e.g., Lasker et al. 2008). The GSC-II is based on $\sim 1''$ resolution scans of photographic plates that were obtained at the Palomar and UK Schmidt telescopes over multiple epochs. The catalog contains the positions, magnitudes, proper motions and classifications (stars and non-stars) of about one billion objects. The GSC-II consists of three pass bands B_J ($\lambda_{\text{eff}} = 0.47 \mu\text{m}$), R_F ($0.64 \mu\text{m}$), and I_N ($0.85 \mu\text{m}$) that cover the optical region of the electromagnetic spectrum. The absolute faint limit of the catalog reaches magnitudes $B_J < 22.5$, $R_F < 20.8$, and $I_N < 19.5$. In this report, the JpgMag, FpgMag, and NpgMag pass bands given in GSC-II are abbreviated to B_J , R_F , and I_N , where the indices J, F, and N comes from the photographic emulsions IIIa-J for the blue, IIIa-F for the red, and IVN for the NIR (see, e.g., Reid et al. 1991).

Because the FGS-Guider is a NIR instrument with a pass band covering $0.6 \mu\text{m}$ to $5 \mu\text{m}$, the GSC-II magnitudes must be converted into the NIR so that we can chose the appropriate reference and guide stars for optimizing the FGS-Guider performance. Chayer et al. (2006) developed color transformations for the conversion of the GSC-II photometric system to the Two Micron All Sky Survey (2MASS) photometric system. 2MASS is a NIR all-sky survey that imaged the sky in three pass bands J ($1.25 \mu\text{m}$), H ($1.65 \mu\text{m}$), and K_S ($2.17 \mu\text{m}$) to limiting magnitudes of 15.8, 15.1, and 14.3, respectively (Skrutskie et al. 2006). The color transformations obtained by Chayer et al. (2006) are given as a set of polynomials of degree one and two.

In this report we present an algorithm for transforming the GSC-II pass bands into the NIR pass bands J , H , and K_S . This algorithm will be used for predicting the magnitudes of the reference and guide stars in the NIR, and ultimately for predicting the electron count rates at the detector (to be provided in a subsequent report). The magnitude-transformation algorithm uses the polynomials developed by Chayer et al. (2006). This report is structured as follows: we first summarize the work of Chayer et al. (2006) in Section 3.0. The uncertainties associated with the transformations are discussed in Section 4.0. The magnitude limits for selecting the reference and guide stars are discussed in Section 5.0. The availability of the GSC-II pass bands is discussed in Section 6.0. Our algorithm is presented in Section 7.0., and the validity of the algorithm applied to fields near the disk of the Galaxy is discussed in Section 8.0.

3.0 Converting GSC-II pass bands into the NIR pass bands

Chayer et al. (2006) analyzed 8 fields of 1° radius at different Galactic latitudes varying from $b = 30^\circ$ to 80° using the GSC-II and 2MASS to derive transformations from the GSC-II (B_J , R_F , I_N) to NIR magnitudes (J , H , K_S)^{*} using color-color diagrams for the 34,204 stars common to both surveys. Figure 1 shows the $(J - B_J)(B_J - I_N)$, illustrating that the data fall along a straight line over a wide range of color. By fitting a straight line

^{*} Kriss & Stys (2003) carried out a similar preliminary analysis based on a 2-square-degree rectangular region centered on the Galactic coordinates $l = 288.9^\circ$ and $b = 62.2^\circ$, but the GSC-II I_N magnitudes were not available at the time of their study.

Check with the JWST SOCCER Database at: <http://soccer.stsci.edu/DmsProdAgile/PLMServlet>

To verify that this is the current version.

to the data (red curve), a relationship between the GSC-II B_J and I_N magnitudes and the 2MASS J magnitude was obtained. Nine color-color diagrams were constructed in order to derive the transformations between the GSC-II pass bands and the 2MASS pass bands, the results of which are summarized in Table 1.

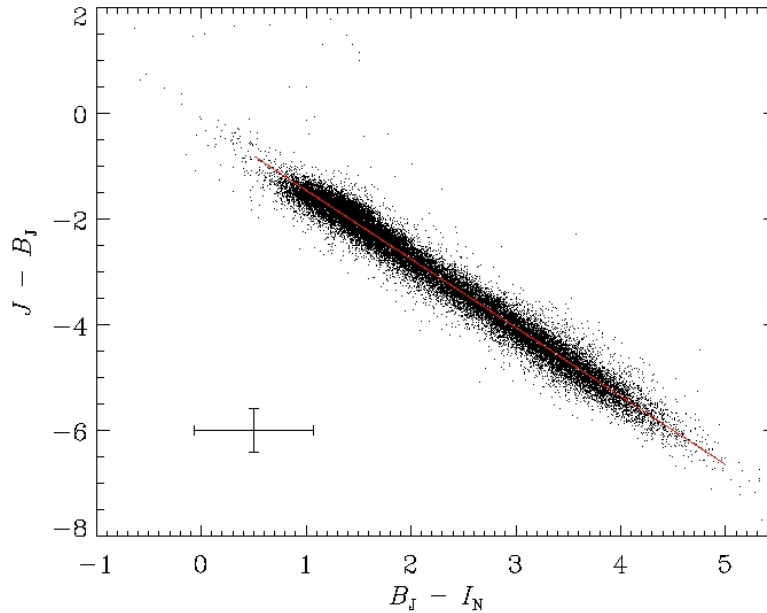


Figure 1- $(J - B_J)(B_J - I_N)$ color-color diagram for stars in common in the GSC-II and 2MASS (black dots). The data correspond to eight combined 1° radius fields that span different Galactic longitudes and latitudes: $(l = 180^\circ, b = 30^\circ)$, $(180^\circ, 35^\circ)$, $(180^\circ, 40^\circ)$, $(180^\circ, 60^\circ)$, $(150^\circ, 80^\circ)$, $(0^\circ, 60^\circ)$, $(90^\circ, 60^\circ)$, and $(270^\circ, 60^\circ)$. The red curve is a straight line that best fits the data. Typical error bars are indicated in the lower left corner of the plot.

Check with the JWST SOCCER Database at: <http://soccer.stsci.edu/DmsProdAgile/PLMServlet>
To verify that this is the current version.

Table 1- Transformations of the GSC-II pass bands (B_J , R_F , and I_N) into the NIR pass bands (J , H and K_S)

Predicted	GSC-II	σ
J	$= B_J - 1.30(B_J - I_N) - 0.15$	0.21
J	$= R_F + 0.01(R_F - I_N)^2 - 1.56(R_F - I_N) - 0.44$	0.25
J	$= B_J - 0.39(B_J - R_F)^2 - 0.96(B_J - R_F) - 0.55$	0.40
J_{AB}	$= J + 0.92$	
H	$= B_J + 0.06(B_J - I_N)^2 - 1.71(B_J - I_N) - 0.10$	0.25
H	$= R_F + 0.25(R_F - I_N)^2 - 2.17(R_F - I_N) - 0.67$	0.33
H	$= B_J - 0.24(B_J - R_F)^2 - 1.66(B_J - R_F) - 0.41$	0.42
H_{AB}	$= H + 1.37$	
K_S	$= B_J + 0.06(B_J - I_N)^2 - 1.78(B_J - I_N) - 0.11$	0.32
K_S	$= R_F + 0.28(R_F - I_N)^2 - 2.35(R_F - I_N) - 0.73$	0.39
K_S	$= B_J - 0.26(B_J - R_F)^2 - 1.70(B_J - R_F) - 0.45$	0.48
$K_{S,AB}$	$= K_S + 1.85$	

4.0 Uncertainties in the Transformations between GSC-II and 2MASS

The accuracy of the transformations for converting the GSC-II pass bands into the 2MASS pass bands depends mainly on the uncertainties of the individual magnitudes. The extinction along the line of sight is another source of uncertainty, but in order to minimize its effect on the transformation, Chayer et al. (2006) considered only data for stars with galactic latitudes $b \geq 30^\circ$ (well above the disk). It is expected that the reddening for these stars is not significant. However, as demonstrated in Section 8, further studies are needed to evaluate the effect of reddening and extinction for stars with $b \leq 30^\circ$. For such regions the use of 2MASS for selecting reference and guide stars is likely to be a better alternative than using the transformations for converting the GSC-II system into the NIR system. Even though 2MASS does not go as deep as GSC-II, the increase in the number of bright stars in the Galactic disk should compensate for the lower sensitivity of 2MASS.

4.1 GSC-II and 2MASS Pass Band Uncertainties

The GSC-II provides the magnitudes B_J , R_F , and I_N with their estimated uncertainties. Figure 2, 3, and 4 show the histograms of the distribution of stars in GSC-II as a function of the stated errors on their magnitudes B_J , R_F , and I_N , respectively. These data were retrieved from 1° radius fields at the galactic coordinates indicated above each panel.

Check with the JWST SOCCER Database at: <http://soccer.stsci.edu/DmsProdAgile/PLMServlet>
To verify that this is the current version.

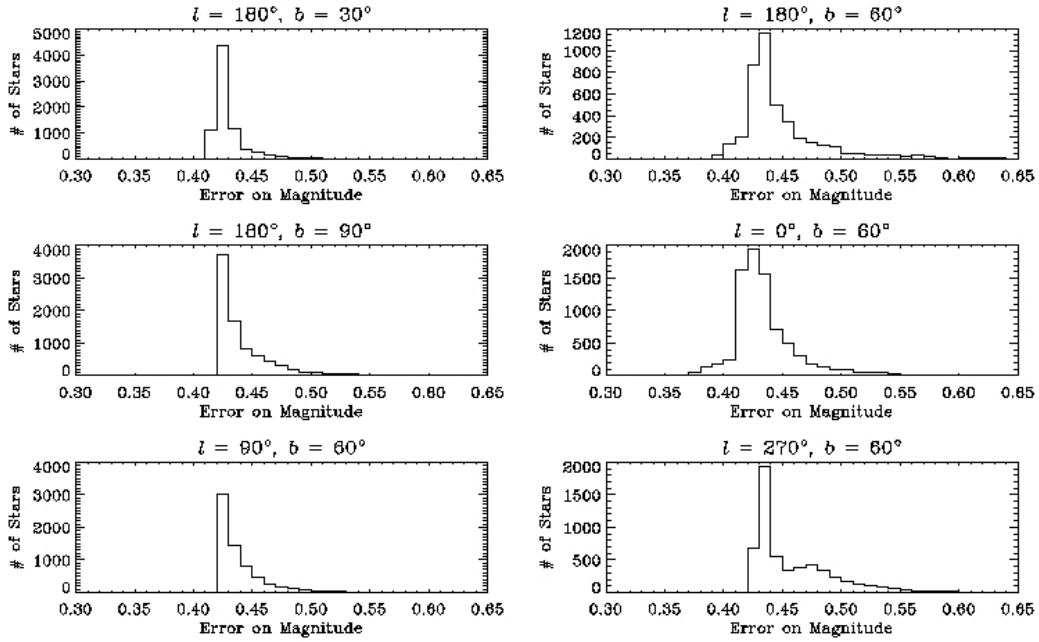


Figure 2- Histograms showing the distribution of stars in GSC-II fields of 1° radius as a function of the errors in their B_J magnitudes (bin size = 0.01). The Galactic longitudes and latitudes are displayed above each panel.

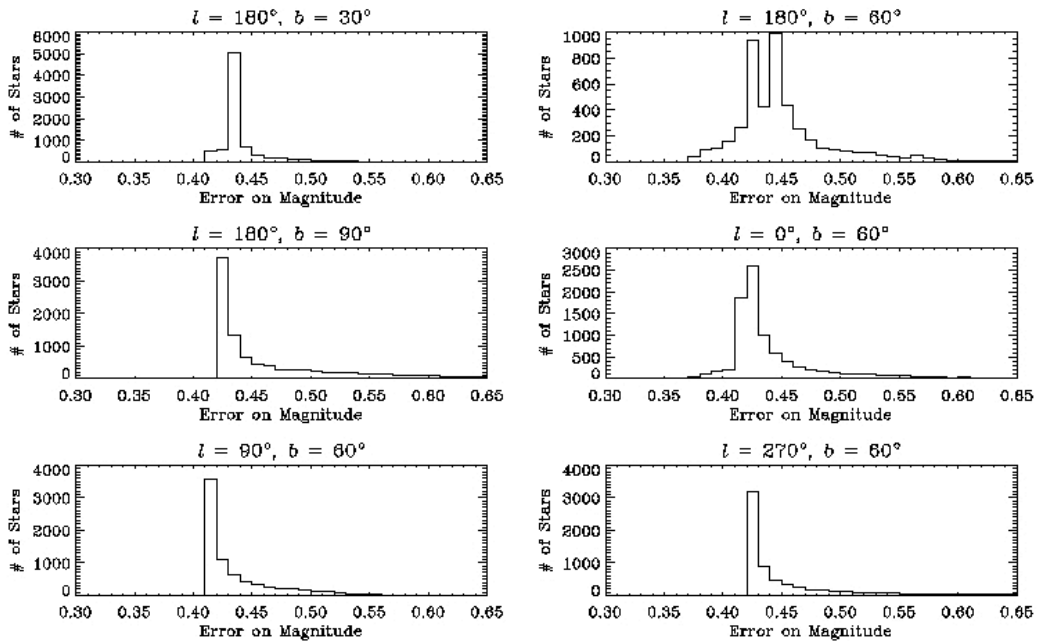


Figure 3- Same as Figure 2, but for the magnitude R_F .

Check with the JWST SOCCER Database at: <http://soccer.stsci.edu/DmsProdAgile/PLMServlet>
 To verify that this is the current version.

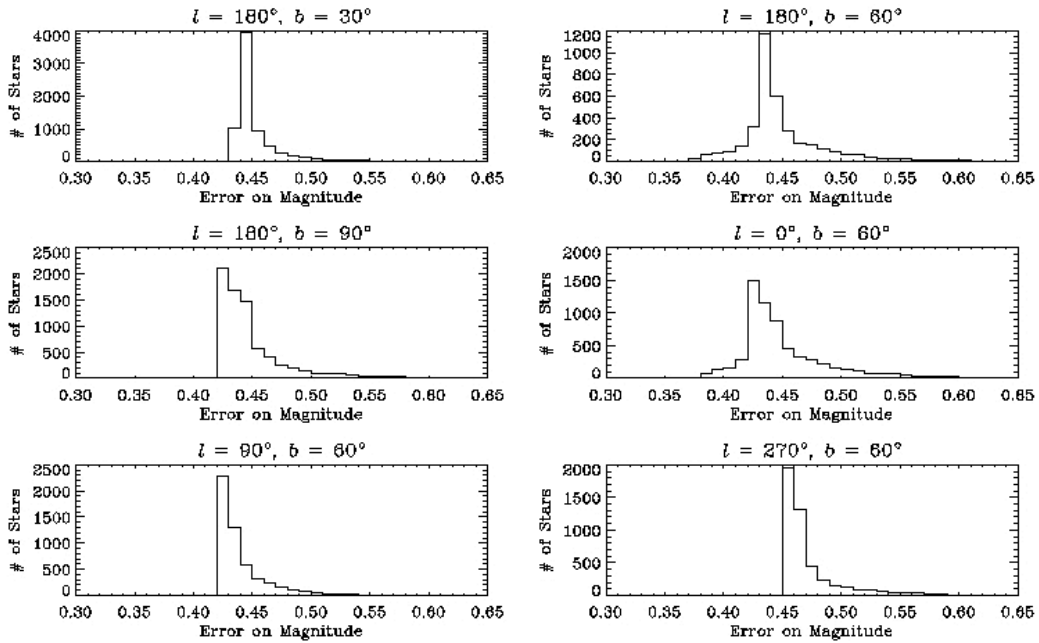


Figure 4- Same as Figure 2, but for the I_N magnitude.

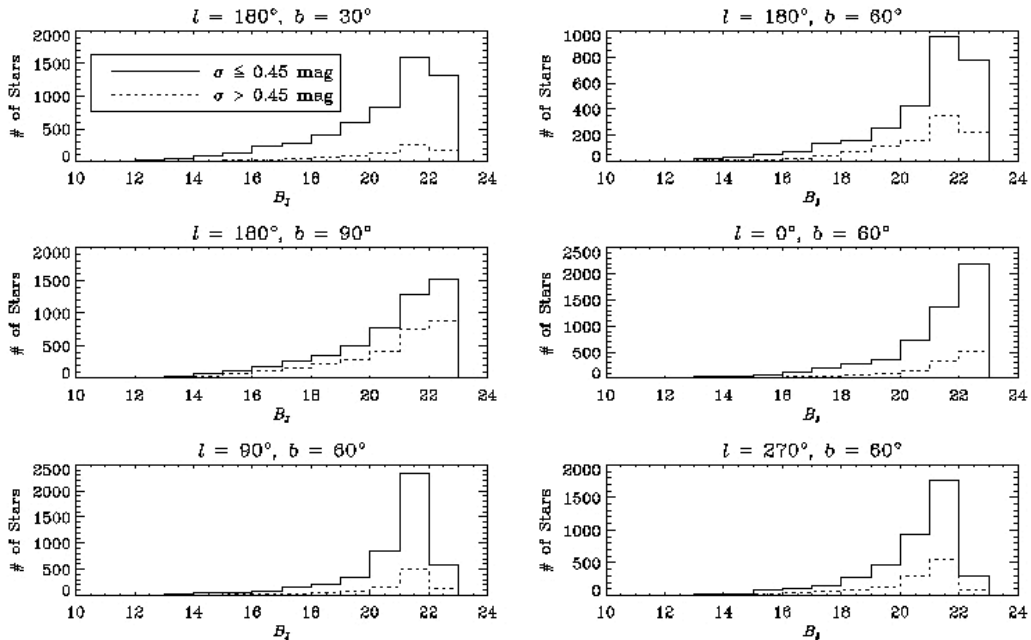


Figure 5- Histograms showing the distribution of the same stars as in Figure 2, but as a function of the B_J magnitude for two ranges of errors on the magnitude ($\sigma \leq 0.45$ and $\sigma > 0.45$).

Check with the JWST SOCCER Database at: <http://soccer.stsci.edu/DmsProdAgile/PLMServlet>
 To verify that this is the current version.

Figure 5 shows the distribution of the same stars as in Figure 2, but as a function of the B_J magnitude for two ranges of errors on the magnitude. The figure shows that the stars with an uncertainty $\sigma \leq 0.45$ mag are not necessarily the brightest stars (e.g., a bright star can have a sizable magnitude error if its image was saturated on the photographic plate). Stars with an uncertainty $\sigma \leq 0.45$ mag have magnitudes from the bright end to the faint end of the catalog. Stars with larger uncertainties have also magnitudes that cover the whole magnitude range.

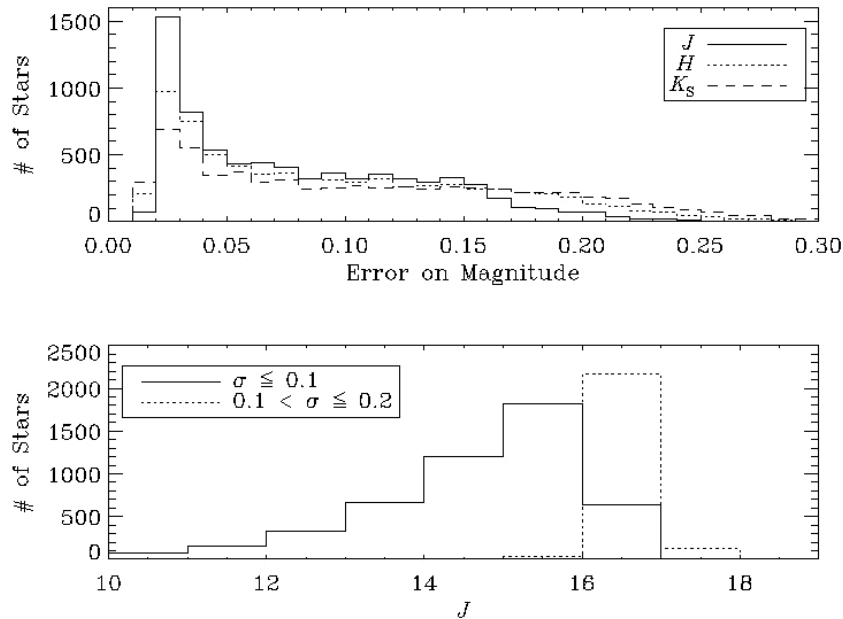


Figure 6- (Upper panel) Histogram showing the distribution of stars in 2MASS as a function of the errors on J , H , and K_S magnitudes. The stars were retrieved from a field of 1° radius located at $l = 180^\circ$ and $b = 35^\circ$. The size of the bin is 0.01 magnitude. (Lower panel) Histograms showing the distribution of the same stars as a function of the J magnitude for two ranges of uncertainties (bin size = 1.0 magnitude).

On the other hand, the uncertainties in the 2MASS pass bands are much lower than the uncertainties in the B_J , R_F , and I_N given in GSC-II. Figure 6 shows the distribution of stars in 2MASS as a function of the uncertainties in J , H , and K_S . The stars were retrieved from a field of 1° radius located at $l = 180^\circ$ and $b = 35^\circ$. The uncertainties in the J , H , and K_S magnitudes vary from 0.01 to 0.35 mag. In the case of the J magnitude, about 66% of stars have an uncertainty $\sigma \leq 0.1$ mag, and about 31% with $0.1 < \sigma \leq 0.2$. The figure also shows (lower panel) that, compared with the GSC-II distribution, the faintest stars have the largest photometric uncertainties. Similar results are observed for the H and K_S magnitudes.

Check with the JWST SOCCER Database at: <http://soccer.stsci.edu/DmsProdAgile/PLMServlet>
To verify that this is the current version.

4.2 Uncertainties in the Predicted J , H , and K_s

The dispersion of data in a color-color diagram as the one illustrated in Figure 1, should have two sources: (1) any spread in the intrinsic correlation between the two colors, and (2) the measurement error in the colors themselves. The cross in the lower left corner of Figure 1 shows the typical error bars associated with the colors $(J - B_J)$ and $(B_J - I_N)$. The individual uncertainties in B_J and I_N come from the uncertainties listed in the GSC-II, and the uncertainties in J come from the uncertainties listed in 2MASS. Because the uncertainties in the J magnitude are much lower than the B_J and I_N magnitudes, the contribution to the errors $\sigma(J - B_J)$ comes essentially from the B_J magnitude. If we take $\sigma(J) = 0.05$ and $\sigma(B_J) = 0.4$, the error in the color $(J - B_J)$ is then

$$\sigma(J - B_J) = (\sigma^2(J) + \sigma^2(B_J))^{1/2} \approx (0.05^2 + 0.40^2)^{1/2} = 0.40. \quad (1)$$

We can also obtain an estimate of the uncertainty on the color $\sigma(J - B_J)$ from the fit in Figure 1. An estimate of the standard deviation from the best fit is given by

$$\sigma^2 = \frac{1}{N-2} \sum (y_i - a - bx_i)^2, \quad (2)$$

where $(N - 2)$ is the number of degrees of freedom, y_i is equal to $(J - B_J)$, a and b are the intercept and slope corresponding to a straight line, and x_i corresponds to $(B_J - I_N)$. The parameters a and b are given in Table 1 ($a = -0.15$; $b = -1.30$). The value of the standard deviation of the data from the fit in Figure 1 is $\sigma = 0.21$. This standard deviation is significantly smaller than the expected uncertainties in the color $(J - B_J)$, which should be close to 0.4 according to the uncertainties provided by GSC-II (see, e.g., Figure 2). This supports the finding of Lasker et al. (2008) that the uncertainties in the B_J magnitudes in GSC-II are overestimated. This is also illustrated in Figure 7, in which the dispersion of the standard deviation from the fit is shown. The standard deviation of this distribution is $\sigma = 0.21$.

We could argue that the tight dispersion of the standard deviation illustrated in Figure 7 may be the result of the cross-correlation between 2MASS and GSC-II producing a list of bright stars, since 2MASS does not go as deep as GSC-II. Further inspection shows, however, that this is not necessarily the case. The upper panel of Figure 8 compares the distribution of stars with B_J , I_N , and J magnitudes that are in common in GSC-II and 2MASS. The stars were retrieved from 8 fields of 1° radius taken at different galactic longitudes and latitudes. The lower panel shows the distribution of the total number of stars in GSC-II with B_J and I_N magnitudes for the same fields. The upper panel shows that a significant number of faint stars in GSC-II *are* in common with 2MASS. Even though there is a large fraction of stars in GSC-II with B_J and I_N magnitudes that have cataloged uncertainties of 0.4 mag, the actual distribution of stars in Figure 1 suggests that the real uncertainties are considerably smaller.

Check with the JWST SOCCER Database at: <http://soccer.stsci.edu/DmsProdAgile/PLMServlet>
To verify that this is the current version.

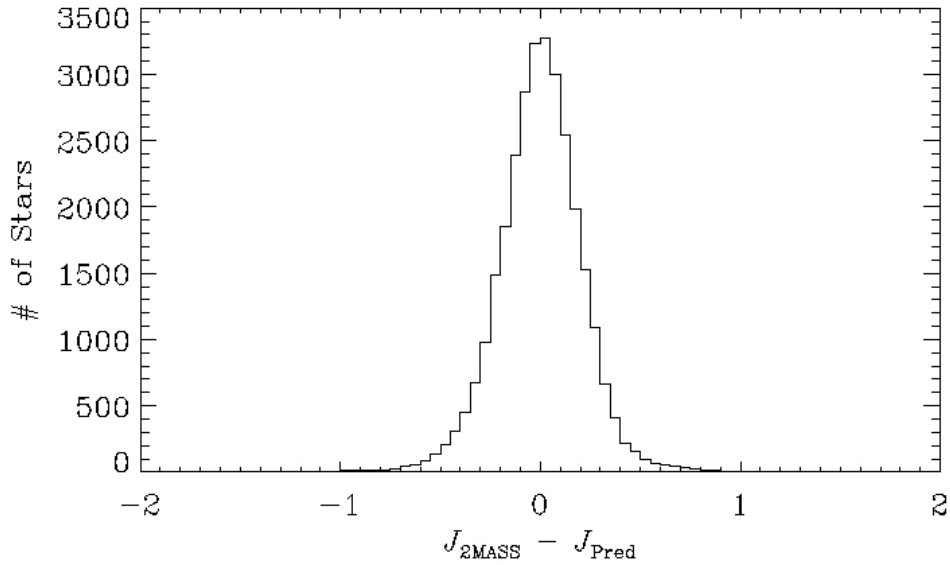


Figure 7- Histogram showing the error distribution for transforming the GSC-II B_J and I_N magnitudes into the 2MASS J magnitude from the polynomial given in Table 1, $J = B_J - 1.30(B_J - I_N) - 0.15$ and illustrated in Figure 1.

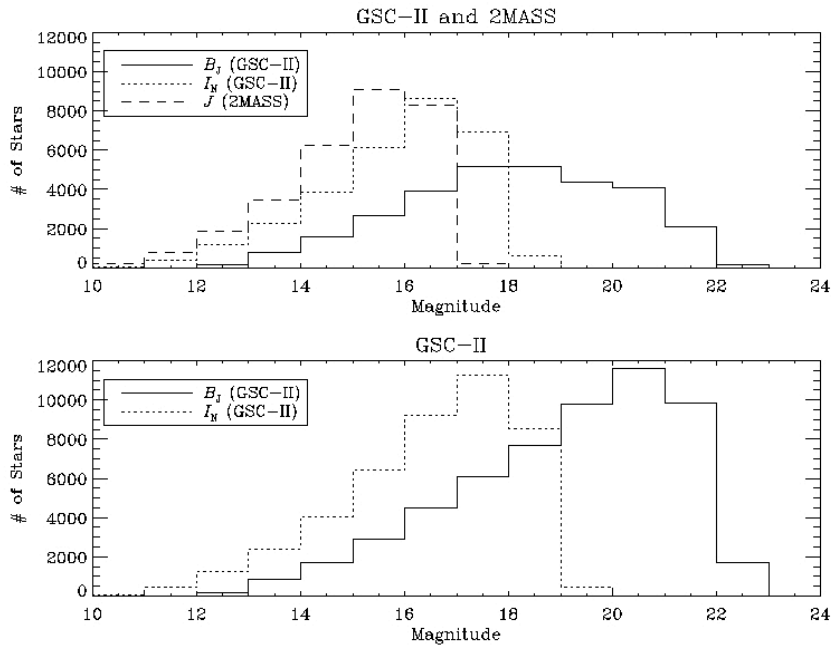


Figure 8- (*Upper panel*) Histogram comparing the distribution of stars in common in both GSC-II and 2MASS for 8 fields of 1° radius. There are 34,204 stars in common. (*Lower panel*) Histogram showing the distribution of the total number of stars in GSC-II for the same 8 fields. There are 63,729 objects classified as stars in these 8 fields.

Check with the JWST SOCCER Database at: <http://soccer.stsci.edu/DmsProdAgile/PLMServlet>
 To verify that this is the current version.

Lasker et al. (2008) obtained similar results when comparing the very accurate photometry of the Sloan Digital Sky Survey (SDSS) Data Release 5 (Adelman-McCarthy et al. 2007) photometric system to the GSC-II photometric system. They transformed the SDSS *ugriz* photometry into the GSC-II pass bands, $B_J R_F I_N$, and compared them to the photographic magnitudes. Table 2 summarizes some of their results from a comparison of a large number of stars in the northern hemisphere ($\sim 40,000$ to $\sim 300,000$ stars). The table gives the standard deviations of the (GSC-II – SDSS) photometric residuals for each GSC-II pass band [$\sigma(\Delta B_J)$, $\sigma(\Delta R_F)$, and $\sigma(\Delta I_N)$] as a function of magnitude in bin sizes of 0.5 mag.

Table 2- GSC-II – SDSS Photometric Residuals ΔB_J , ΔR_F , and ΔI_N

B_J, R_F, I_N	$\sigma(\Delta B_J)$	$\sigma(\Delta R_F)$	$\sigma(\Delta I_N)$
13.5–14.0		0.16	0.17
14.5–15.0	0.42	0.13	0.13
15.5–16.0	0.19	0.12	0.14
16.5–17.0	0.17	0.12	0.15
17.5–18.0	0.17	0.13	0.19
18.5–19.0	0.16	0.15	0.26
19.5–20.0	0.18	0.22	
20.5–21.0	0.22		
21.5–22.0	0.27		

Data adapted from Lasker et al. (2008)

Table 2 shows that the GSC-II magnitudes can achieve a precision of $\sigma(\Delta B_J) \cong 0.16$, $\sigma(\Delta R_F) \cong 0.12$, and $\sigma(\Delta I_N) \cong 0.13$. The precision decreases for bright (saturated) stars, and for stars near the faint limit of the plates. The precision in those cases can reach ~ 0.20 – 0.25 mag. The standard deviations in Table 2 show similar values to the ones we obtained when comparing GSC-II and 2MASS, and suggest once again that the uncertainties in B_J , R_F , and I_N magnitudes that are listed in GSC-II are overestimated.

Our sources of errors on the predicted NIR magnitudes not only come from the quality of the data retrieved from GSC-II and 2MASS, but also from the quality of the fit of the color-color diagrams. Figure 1 shows that the fit of the distribution of stars in the color-color diagram $(J - B_J)(B_J - I_N)$ is very good. In this case, for instance, the uncertainty on the predicted J magnitude comes essentially from the quality of the data. On the other hand, fitting data in the color-color diagram $(J - B_J)(B_J - R_F)$ with a polynomial may not give results as accurate as those for the color-color diagram $(J - B_J)(B_J - I_N)$. Figure 9 shows that the distribution of stars in the $(J - B_J)(B_J - R_F)$ diagram has a bulge in the region where $1.7 \leq (B_J - R_F) \leq 2.7$ and $4.0 \leq (J - B_J) \leq 6.0$. The best fit to the data (red curve) does not reproduce the data very well in the region where the bulge is present. This means that for stars with color in the range $1.7 \leq (B_J - R_F) \leq 2.7$, the determination

Check with the JWST SOCCER Database at: <http://soccer.stsci.edu/DmsProdAgile/PLMServlet>
To verify that this is the current version.

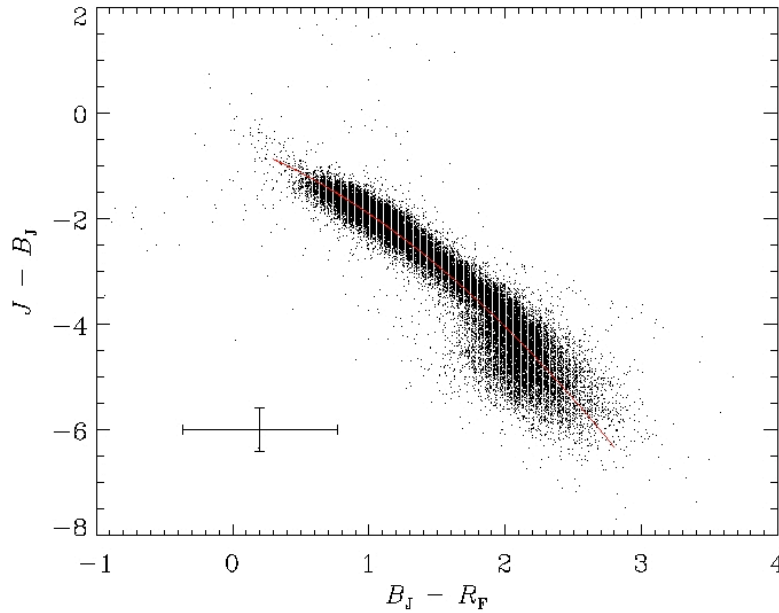


Figure 9- Same as Figure 1, but for the $(J - B_J)(B_J - R_F)$ color-color diagram.

of the J magnitude will not be very accurate.

The quality of the fit can be assessed with the assistance of Figure 10, which illustrates the distribution of the deviation from the best fit shown in Figure 9. Figure 10 shows that the distribution is not as tight as the one illustrated in Figure 7. The tails of the distribution, in particular, show that the errors on the predicted J magnitudes can be quite large. The extended tails in Figure 10 are the result of the poor fit in the range $1.7 \leq (B_J - R_F) \leq 2.7$. The standard deviation of the data is $\sigma = 0.40$. This value is twice the one for the best fit that is illustrated in Figure 1 ($\sigma = 0.21$).

The standard deviation from the best fits, when fitting the distribution of stars in a color-color diagram, can be used for assessing the transformations given in Table 1. The last column in Table 1 gives the standard deviation from the best fit for each transformation that we derived when fitting color-color diagrams involving data from GSC-II and 2MASS. Their values vary from 0.21 to 0.48. Based on these values we can specify which transformations are going to provide the most accurate NIR magnitudes. Table 1 shows that the best transformations for deriving the J , H , and K_S magnitudes are those that use the B_J and I_N magnitudes. Transformations using the R_F and I_N magnitudes provide NIR magnitudes that are somewhat less accurate. Finally, using only the B_J and R_F magnitudes provides the least accurate NIR magnitudes.

Check with the JWST SOCCER Database at: <http://soccer.stsci.edu/DmsProdAgile/PLMServlet>
To verify that this is the current version.

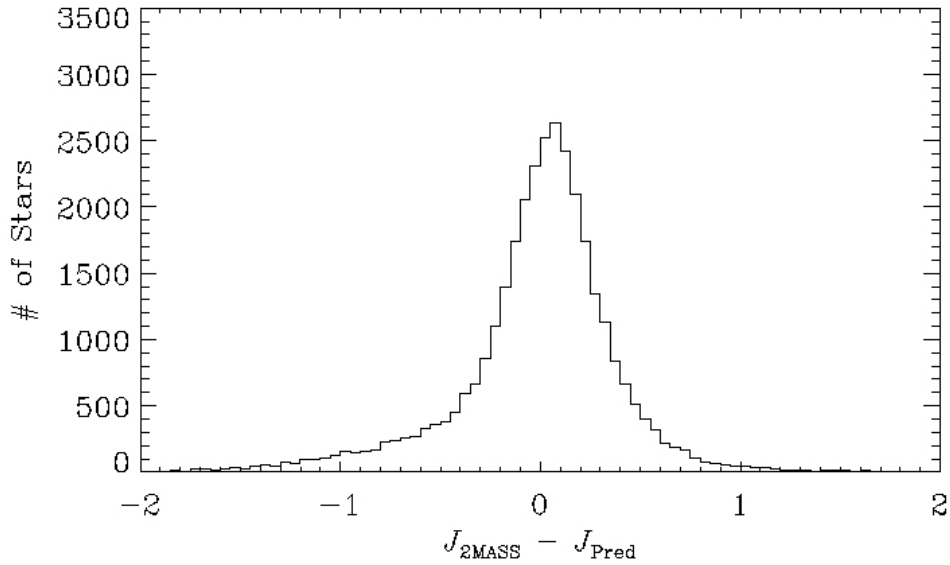


Figure 10- Same as Figure 7, but for transforming the GSC-II B_J and R_F magnitudes into the 2MASS J magnitude from the polynomial given in Table 1 $J = B_J - 0.39(B_J - R_F)^2 - 0.96(B_J - R_F) - 0.55$ and illustrated in Figure 9.

5.0 Magnitude Limits

The FGS-Guider is sensitive to light in the NIR from $0.6 \mu\text{m}$ to $5 \mu\text{m}$. The guider’s faint limiting magnitude and required field of view (FOV) is derived from requirement MR-365 (ISIM-265), which stipulates that *no single point failure in the FGS shall decrease the probability of acquiring a guide star below 90%*, along with the requirement that the 16 Hz guide star centroids have a noise equivalent angle less than $3.5 \text{ mas } 1\text{-}\sigma/\text{axis}$. The guide star faint magnitude limit is derived from an analysis that convolves the OTE and FGS optical throughputs and detector sensitivity with the spectral energy distribution of stars of various spectral types to determine the electron count rate at the detector (which then determines the accuracy with which the guide star’s position can be measured). Current estimates put the faint magnitude limit at $J_{AB} = 19.4$ for an M0 star ($J_{AB} < 19.9$ for an A0 star). On the other hand, the reference stars used for the Identification function can be fainter, both because the Identification exposure time is ~ 16 times longer than the Fine Guide exposure time, and there is no formal requirement for an accurate centroid measurement. It is expected that the FGS will “see” objects in the Identification image down to $J_{AB} \sim 23.5$ (note that GSC-II will not contain these faint stars, so they will not be used as reference stars in the Identification function). The guide stars and reference stars may be as bright as $J_{AB} \approx 13$. In summary, the bright and faint magnitude limits for a

Check with the JWST SOCCER Database at: <http://soccer.stsci.edu/DmsProdAgile/PLMServlet>
To verify that this is the current version.

guide star are: $13 \leq J_{AB} \leq 19.5$. Reference stars have the same bright limit but have no effective faint limit.*

6.0 Availability of GSC-II B_J , R_F , and I_N Magnitudes

Inspection of GSC-II shows that a given object may not have magnitudes available in all three pass bands. This can occur for a variety of reasons (see Lasker et al, 2008), but nonetheless can present a difficulty for transforming into the NIR magnitudes. Table 3 (from Chayer et al. 2006) illustrates that approximately 1/3 of the GSC-II stars do not have both a B_J and I_N magnitude, which implies that the less accurate $J_{AB}(B_J, R_F)$ transformation must be applied instead of the preferred $J_{AB}(B_J, I_N)$. Stars with just one GSC-II magnitude should not be selected as guide stars (they may be useful reference stars, but the magnitude transformation algorithm is still TBD).

Galactic Coord.	Number of stars								
	Total	$B_J, R_F, \text{ and } I_N$	B_J, R_F	B_J, I_N	R_F, I_N	B_J	R_F	I_N	No B_J, R_F, I_N
180° 30°	9018	7197	537	21	16	383	335	374	155
180° 35°	7811	6027	302	6	194	366	482	270	164
180° 40°	7201	5461	556	5	17	582	202	239	139
180° 50°	7337	4701	726	2	23	1062	284	409	130
180° 55°	6818	4016	1383	0	14	699	337	277	92
180° 60°	5155	3600	645	1	32	424	133	244	76
180° 65°	5750	3699	519	4	84	544	393	394	113
180° 70°	6423	3671	394	3	237	949	646	429	94
150° 80°	4669	3399	238	0	162	224	232	296	118
0° 60°	14100	5728	6564	5	63	838	525	247	130
90° 60°	8331	5138	1280	29	69	865	655	164	131
180° 60°	5155	3600	645	1	32	424	133	244	76
270° 60°	7444	4638	890	2	78	942	412	419	63

Table 3- Number of stars for which GSC-II magnitudes are available in three pass bands (B_J , R_F , and I_N), two pass bands (B_J and R_F ; B_J and I_N ; R_F and I_N), and one pass band (B_J ; R_F ; I_N).

7.0 Algorithm for converting GSC-II into 2MASS

The algorithm that we suggest for transforming the GSC-II pass bands into the NIR is based on the transformations that are listed in Table 1. As we have shown, some transformations are more accurate than others. Therefore, we need to select the transformations that give the most accurate results for a given set of GSC-II magnitudes B_J , R_F , and I_N . Based on our discussion in Section 4.0, we suggest the following algorithm for deriving the J_{AB} , H_{AB} , and $K_{S,AB}$ magnitudes from the GSC-II B_J , R_F , and I_N magnitudes.

* The bright limit has not been fully analyzed. The issue is tolerance of saturation during Identification (which applies to the guide star and reference stars) and Acquisition (guide star only) as these involve longer exposure times than Fine Guide.

Check with the JWST SOCCER Database at: <http://soccer.stsci.edu/DmsProdAgile/PLMServlet>
To verify that this is the current version.

Read GSC-II magnitudes B_J , R_F , and I_N

If (B_J and I_N are available) **then** compute $J_{AB}(B_J, I_N)$, $H_{AB}(B_J, I_N)$, and $K_{S,AB}(B_J, I_N)$ transformations, where

$$J_{AB}(B_J, I_N) = B_J - 1.30(B_J - I_N) + 0.77$$

$$H_{AB}(B_J, I_N) = B_J + 0.06(B_J - I_N)^2 - 1.71(B_J - I_N) + 1.27$$

$$K_{S,AB}(B_J, I_N) = B_J + 0.06(B_J - I_N)^2 - 1.78(B_J - I_N) + 1.74$$

Else if (R_F and I_N are only available) **then** compute $J_{AB}(R_F, I_N)$, $H_{AB}(R_F, I_N)$, and $K_{S,AB}(R_F, I_N)$ transformations, where

$$J_{AB}(R_F, I_N) = R_F + 0.01(R_F - I_N)^2 - 1.56(R_F - I_N) + 0.48$$

$$H_{AB}(R_F, I_N) = R_F + 0.25(R_F - I_N)^2 - 2.17(R_F - I_N) + 0.70$$

$$K_{S,AB}(R_F, I_N) = R_F + 0.28(R_F - I_N)^2 - 2.35(R_F - I_N) + 1.12$$

Else if (B_J and R_F are only available) **then** compute $J_{AB}(B_J, R_F)$, $H_{AB}(B_J, R_F)$, and $K_{S,AB}(B_J, R_F)$ transformations, where

$$J_{AB}(B_J, R_F) = B_J - 0.39(B_J - R_F)^2 - 0.96(B_J - R_F) + 0.37$$

$$H_{AB}(B_J, R_F) = B_J - 0.24(B_J - R_F)^2 - 1.66(B_J - R_F) + 0.96$$

$$K_{S,AB}(B_J, R_F) = B_J - 0.26(B_J - R_F)^2 - 1.70(B_J - R_F) + 1.40$$

Else (only 1 pass band available) **then** do not use the star,

Endif

We suggest that the uncertainties in the predicted J_{AB} , H_{AB} , and $K_{S,AB}$ magnitudes should correspond to the standard deviations given in Table 1. For instance, the transformation $J_{AB}(B_J, I_N)$ should be assigned an uncertainty $\sigma = 0.21$ mag.

Once we have estimated the J_{AB} , H_{AB} , and $K_{S,AB}$ magnitudes, we need to determine the FGS-Guider electron count rates. The expected FGS-Guider electron count rates for a given guide star and its associated reference stars consists of integrating the spectral energy distribution for each star over the FGS-Guider throughput. This result is then integrated for obtaining the total signal level in electron per second. The spectral energy distribution is determined by using the estimated J_{AB} , H_{AB} , and $K_{S,AB}$ magnitudes. The FGS-Guider throughput has been determined by ComDev and is now available (see, e.g., ComDev Technical Note: JWST FGS Guider Throughput, 2008). We are now in a position to derive the algorithm for predicting the FGS-Guider count rates. This algorithm will be presented in a subsequent report.

Check with the JWST SOCCER Database at: <http://soccer.stsci.edu/DmsProdAgile/PLMServlet>
To verify that this is the current version.

8.0 Application of the High Latitude Transformations to Fields Near the Disk

The GSC-II to NIR magnitude transformations specified in the previous section were derived using 2MASS data from fields at high Galactic latitudes. As expected (Chayer et al. 2006), very little variation in the goodness of fit of these transformations was seen over the 13 widely separated fields that were studied by those authors. This is a fortunate result since it implies that extinction and reddening effects do not need to be modeled on a local scale for fields outside of the Galaxy's disk ($|b| > 30^\circ$).

In this section we explore the application of the transformations outlined in Section 6 to a field in Cygnus OB2, a star forming region in the disk of the Galaxy, 1.7 kpc distant, known to suffer significant reddening and extinction. Figure 11 illustrates the color-color diagram for stars in this region (J, H, K are from 2MASS, B_J, R_F, I_N are from GSC-II). Compared to the high latitude field in Figure 1, these diagrams show much greater dispersion, which will result in larger errors for predicted NIR magnitudes (1.5 magnitudes). Moreover, these diagrams are not likely to be representative of other regions in the Galaxy's disk. Fortunately the 2MASS survey is sufficiently deep to achieve an adequate areal density of stars to support JWST operations given the size of the FGS FOV. It is recommended that the guide star selection system use 2MASS if we are able to integrate it into the GSC-II for JWST operations, especially for low latitude fields that are subject to locally varying levels of reddening and extinction.

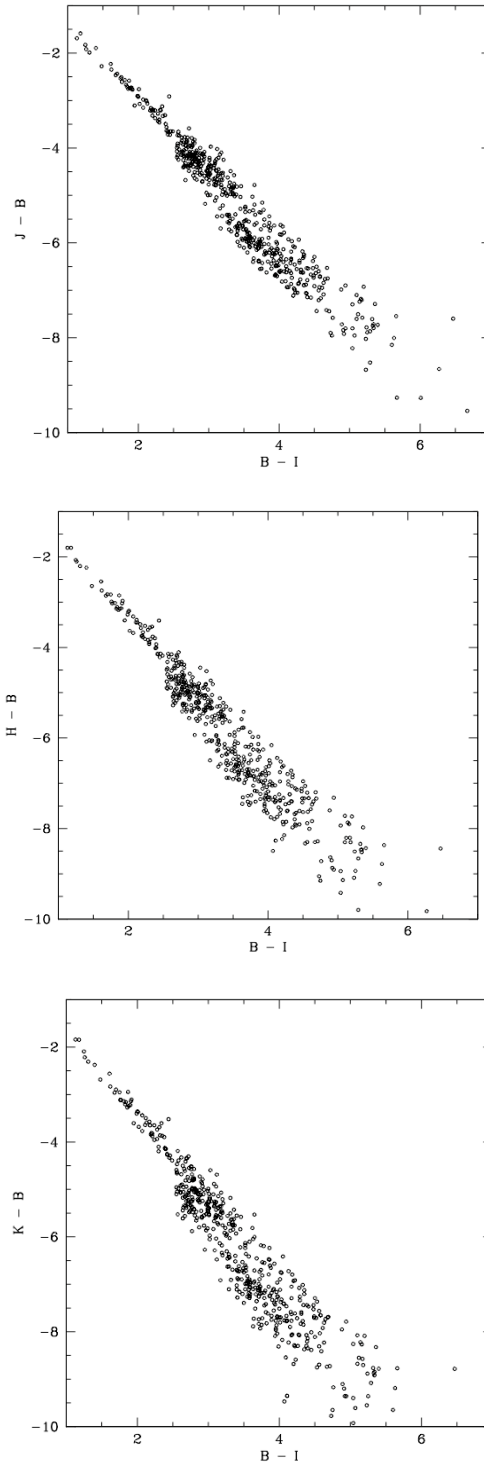


Figure 11. Color-color diagrams for GSC-II and 2MASS magnitudes for Cyg OB2 indicates that the high latitude transformation do not accurately apply for regions in the disk (compare to Figure 1).

Check with the JWST SOCCER Database at: <http://soccer.stsci.edu/DmsProdAgile/PLMServlet>
To verify that this is the current version.

9.0 References

Adelman-McCarthy, J. K., and 153 coauthors 2007, *The Fifth Data Release of the Sloan Digital Sky Survey*, *Astrophysical Journal Supplement Series*, 172, 634.

ComDev Team, 2008, *JWST FGS Guider Throughput*, Technical Note, Document Number: TNO/CSA/51221/022.

Chayer, P., Stys, J., Nelan, E. P., and Kriss, G. A. 2006, *Extrapolating the Properties of the Guide Star Catalog into the Near Infrared*, JWST-STScI-000920.

Kriss, G. A., & Stys, J. 2003, *The Suitability of Guide Star Catalog 2 (GSC-2) as a Source for JWST Guide Stars*, JWST-STScI-000400.

Lasker, B. M., Lattanzi, M. G., McLean, B. J., Bucciarelli, B., Drimmel, R., Garcia, J., and 20 coauthors, 2008, *The Second Generation Guide Star Catalog: description and properties*, submitted to the *Astronomical Journal*.

Reid, I. N., et al. 1991, *The Second Palomar Sky Survey*, *Publication of the Astronomical Society of the Pacific*, 103, 661.

Skrutskie, M. F., et al. 2006, *The Two Micron All Sky Survey (2MASS)*, *Astronomical Journal*, 123, 485.

Check with the JWST SOCCER Database at: <http://soccer.stsci.edu/DmsProdAgile/PLMServlet>
To verify that this is the current version.